Optical transitions from the lowest to higher exciton and biexciton Rydberg states in CuCl

K. Miyajima,* K. Sakaniwa, and M. Sugawara

Department of Applied Physics, Graduate School of Science, Tokyo University of Science, 6-3-1 Niijuku Katsusika-ku, Tokyo 125-8585, Japan

(Received 10 March 2016; revised manuscript received 24 October 2016; published 28 November 2016)

We measured the optical transitions due to the internal energy levels of an exciton and biexciton in a CuCl single crystal using pump-probe spectroscopy. The transient absorption bands due to the transitions from the $1s$ to $2p$ and from the $1s$ to $3p$ exciton states were observed at 3 K, which is consistent with their reported energies. Simultaneously, the transient absorption peak due to the biexciton was observed, which corresponds to a transition from the lowest state (composed of two $1s$ excitons) to higher states (composed of $1s$ and $2p$ excitons). The value of the observed biexciton peak energy was reasonable considering the hydrogen molecule orbitals and the electron-to-hole effective mass ratio. In addition, the transient absorption peaks were broadened at 77 K, because of the increase in the homogeneous width of the $2p$ exciton state. The transient absorption spectrum was almost completely determined by this width. Our findings are of importance with regard to the optical phenomena in the infrared region related to the quantum coherence of excitons and biexcitons in semiconductors.

DOI: 10.1103/PhysRevB.94.195209

I. INTRODUCTION

An exciton is an electron-hole pair bound through Coulomb interaction that has internal energy levels determined by relative motion between the electron and hole; these energy levels are similar to the Rydberg series of a hydrogen atom [1]. Optical research on the exciton has primarily focused on the lowest $1s$ state, because the most noticeable absorption band and luminescence are obtained for this state. However, the optical transitions between the lowest to higher exciton energy states are advanced topics as regards research on the optical properties related to the exciton coherence of semiconductors. This is because an exciton is an ideal quantum system in a semiconductor. To date, a small number of studies related to transitions between the Rydberg energy levels of the exciton have been reported. In the case of Cu_2O crystals, various Lyman-spectroscopy-based reports have been published, in which the absorption from the lowest $1s$ to the higher Rydberg states [2,3], the alternating-current (ac) Stark effect on the exciton under a strong electromagnetic field resonant to the transition between the $1s$ to $2p$ states [4], and the Rabi oscillation between the $1s$ and $2p$ states [5] were examined. In addition, the fine energy levels of the higher Rydberg states have recently been investigated [6]. As regards materials other than Cu_2O, observation of the ac Stark effect induced by the transition energy between the exciton Rydberg states in the terahertz range has been reported, e.g., for GaAs/AlGaAs multiquantum wells [7,8].

On the other hand, the fine energy levels of the biexciton, which is a bound two-exciton pair, have not been resolved. The lowest energy of the biexciton is less than twice the exciton energy, as a result of the biexciton binding energy. The biexciton binding energy has been reported as being a function of the electron-to-hole effective mass ratio [9–11], and the existence of biexcitons in all semiconductors is expected. The lowest biexciton state is composed of two $1s$ excitons, and corresponds to the ${}^1\Sigma_g^+$ bonding orbital of the hydrogen molecule [12]. However, the other higher-energy levels related to the $1s$ and $2s$, and $1s$ and $2p$ bonding states, which correspond to the ${}^3\Sigma_g^+$ and ${}^1\Sigma_u^+$ orbitals of a hydrogen molecule [12], respectively, have not been revealed. In this paper, these energy levels are denoted ($1s$, $2s$) and ($1s$, $2p$), respectively. Investigation of the optical transitions between the internal energy levels of the biexciton would facilitate improved understanding of interactions between multiexcitons.

The realization of well-designed semiconductor nanostructures, e.g., quantum wells (QWs), quantum wires (QWRs), and quantum dots (QDs), has enhanced the importance of the study of optical transition processes for quantized energy levels originating in intrabands, which are induced by quantum confinement effects. Their transition processes can be applied to novel optical devices in the infrared region, e.g., quantum cascade lasers [13] and photodetectors [14]. Such studies have focused on the electron or hole transitions, in which the quantum confinements to excitons in nanostructures have been classified into "individual confinement regimes," because the nanostructure is smaller than the exciton effective Bohr radius. On the other hand, for nanostructures deemed to exhibit the "exciton confinement effect," where the exciton effective Bohr radius is smaller than the nanostructures, the transitions between the exciton Rydberg energy levels are important. However, as the higher Rydberg exciton states have extended wave functions compared to that of the lowest $1s$ exciton state, the transition energies from the $1s$ to $2p$ states are dependent on the size of the nanostructure [15]. From this perspective, not only the quantized energy levels of the electron and hole, but also the Rydberg energy states of the exciton are important with regard to the infrared optical properties. Furthermore, the higher excited levels of the biexciton in a QD should be examined, because it is expected that a strong correlation between two excitons induces specific energy levels and transition dynamics different from those of the bulk crystal.

CuCl is an appropriate material for the aforementioned research, because of its large exciton Rydberg energy of 197 meV [16] and biexciton binding energy of 32 meV [17–19]. The Rydberg s series of the exciton in CuCl has been reported based on one-photon absorption measurement, whereas that for the p series has been obtained by considering

*miyajima@rs.tus.ac.jp

the photoluminescence excitation (PLE) spectrum of the I_1 line. The latter is attributed to the exciton bound to the neutral acceptor through the two-photon excitation process [16]. On the other hand, the lowest biexciton energy in CuCl has been evaluated clearly using both resonant two-photon absorption [17,18] and resonant two-photon Raman scattering [19,20]. However, the higher energy levels related to the Rydberg excited states have not been examined, apart from in our previous reports [21]. The infrared transient absorption (IRTA) measured using pump-probe spectroscopy is a useful tool for revealing the optical transitions between the internal energy levels of the exciton and biexciton. For CuCl QDs embedded in a NaCl crystal, an increase in the transition energy from the $1s$ to $2p$ exciton states has been reported, which was experimentally obtained by decreasing the effective dot radius [22]. In addition, we have examined the IRTA due to the transition from the lowest ($1s$, $1s$) state to the higher ($1s$, $2p$) biexciton state with resonant two-photon excitation of the biexcitons [20]. Moreover, the IRTA spectra of 3-μm-thick CuCl films grown on CaF_2 substrate have been reported [21]. In that study, under resonant two-photon absorption of the biexcitons, the IRTA of the biexciton and exciton were obtained. The biexciton and exciton contributions to the IRTA were determined based on their time profiles, and the transition due to the exciton from the $1s$ to the $2p$ and $3p$ states and that due to the biexciton from the ($1s$, $1s$) to the ($1s$, $2p$) state were assigned. However, the energy structures obtained from the IRTA spectra were ambiguous because of the low signal-to-noise ratios. To clarify the excited levels of the biexciton in a semiconductor bulk crystal and to examine the effects of confinement in nanostructures on these levels, unambiguous transient absorption spectra attributed to both excitons and biexcitons are necessary.

In this study, we successfully obtain IRTA spectra exhibiting the energy structures due to the exciton and biexciton Rydberg states in a CuCl single crystal at 3 K. The IRTA components attributed to the excitons and biexcitons are separated based on decay times, which are obtained from the IRTA time profiles. Compared to the previous experiment on CuCl films, the stability of the light intensity is improved and the spectral width is reduced, which results in clarification of the IRTA spectra. The transition energy of the lowest to the higher excited states is reasonable considering the molecular orbitals of a hydrogen molecule. In addition, we find that the fine structure of the IRTA spectrum disappears as the temperature increase because of the broadening of the homogeneous width of the $2p$ exciton band.

II. EXPERIMENTAL METHOD

The sample used in this study was a CuCl single crystal grown from CuCl powders of 5N purity in an Ar gas atmosphere (0.3 atm) using a vapor phase transport method. The source of the CuCl powders was heated to 410 °C for 2 weeks. As a result, CuCl plates with thicknesses of several tens of micrometers were grown. The sample surface was a (111) plane.

The photoluminescence (PL) spectra under weak band-to-band excitation were measured in order to evaluate the sample quality. The excitation-light source was a continuous

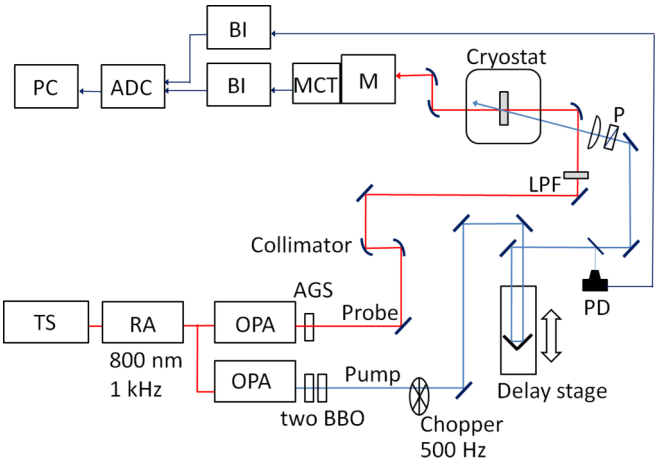

FIG. 1. Optical system used for IRTA measurements. TS, RA, and OPA indicate a mode-locked Ti:sapphire laser, a regenerative amplifier, and an optical parametric amplifier, respectively. AGS and BBO are $AgGaS_2$ and β-BaB_2O_4 crystals, respectively. PD and MCT indicate a photodiode and a photovoltaic HgCdTe detector, respectively. P and LPF represent a polarizer and a low-pass filter, respectively. M, BI, and ADC are a monochromator, a boxcar integrator, and an analog-digital converter, respectively.

wave diode-pumped solid-state (DPSS) laser with 355-nm wavelength. The IRTA was obtained via pump-probe spectroscopy using dual optical parametric amplifiers pumped by a regenerative amplifier (repetition rate: 1 kHz; pulse duration: ∼3 ps; spectral width: ∼2.5 meV). Figure 1 shows the optical system used for the IRTA measurements. The pump light was obtained from the fourth harmonic light of the signal beam, which was generated using two β-BaB_2O_4 crystals, from one optical parametric amplifier. The photon energy was tuned to the resonant two-photon absorption energy of the biexciton. The pump-light repetition rate was reduced to 500 Hz using an optical chopper synchronized with the laser system. The PL spectra were measured using a spectrometer (focal length: 500 mm; grating: 2400 g/mm) equipped with a charge-coupled device (CCD). The probe light was obtained via differential frequency generation of the signal and idler beams from another optical parametric amplifier, which was achieved using an $AgGaS_2$ crystal. The probe-light photon energy was varied in the 140−205-meV range. The transmitted probe light was measured using a liquid-N_2-cooled HgCdTe (MCT) detector positioned after a monochromator (focal length: 150 mm; grating: 150 g/mm). The light intensities of the single pulses were obtained using a boxcar integrator. The sample was fixed to a holder in a cryostat, and the temperature T was changed from 3 to 77 K. Figure 2 shows the pump-probe spectroscopy energy scheme. The lowest-energy biexcitons were generated directly by the pump light through a resonant two-photon excitation process. The excitons are thought to have originated from a biexciton relaxation process. The transitions to the biexciton and exciton excited states were induced simultaneously by the probe light. The exciton and biexciton contributions were classified based on the time evolution of the IRTA spectra.

Furthermore, the PLE spectra of the I_1 emission were measured in order to obtain the absorption bands of the higher

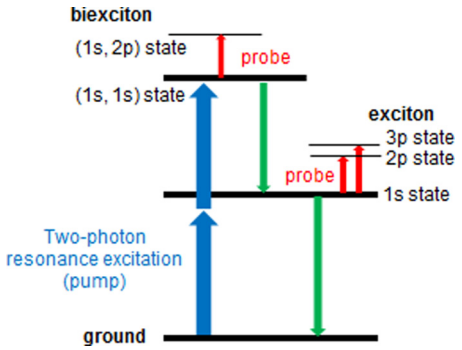

FIG. 2. Pump-probe spectroscopy energy scheme used in this study. The wide and narrow upward arrows indicate the pump and probe lights, respectively, whereas the downward arrows indicate the biexciton and exciton relaxation. The pump-light photon energy was tuned to the resonant two-photon absorption energy of the biexcitons. The probe-light photon energy was varied to facilitate observation of the absorption from the lowest to the higher excited states.

Rydberg exciton states. The excitation light was obtained via second harmonic generation of a signal beam from one optical parametric amplifier, and the photon energy was varied continuously from 1.57 to 1.72 eV. The excitons were generated through a two-photon absorption process. The sample T was varied from 3 to 50 K.

III. RESULTS AND DISCUSSION

A. PL spectra of sample

PL measurements were performed in order to evaluate the impurity levels and to determine the appropriate excitation density for the IRTA measurement. Figure 3(a) shows the T dependence of the PL spectra under band-to-band weak excitation. At low T, the I_1 line, which was attributed to the excitons trapped in neutral acceptors, was strongest. The weak PL band appearing around the I_1 line was attributed to shallow impurity levels. The PL band denoted by E_x in Fig. 3(a), which appeared at 3.2040 eV, was attributed to the free excitons; this is almost consistent with the transverse exciton energy value of 3.2023 eV at 2 K [23]. The triplet exciton was optically forbidden [24]. We suggest that, in this experiment, the PL of the triplet exciton was observed at 3.2018 eV, because of unexpected stresses resulting from the attachment to the sample holder. When T was increased, the strongest I_1 line and the other PL bands and PL lines decreased as a result of shallow impurities. In contrast, the PL intensity of the free exciton increased up to 70 K before decreasing. The peak energies of all the bands shifted to higher values, reflecting the change in the band-gap energy [25]. At 77 K, the E_x band and the 2LO (LO: longitudinal optical) phonon sideband were dominant, and the I_1 line disappeared.

The T dependence of the PL spectra under the resonant two-photon absorption of the biexcitons is shown in Fig. 3(b). The excitation density was $43\mu J/cm^2$, and the excitation photon energy was tuned to the resonant energy by considering the change in the band-gap energy. Specific troughs in the scattered excitation-light spectrum are labeled "Excitation" in the figure, and are indicated by arrows. The spectral width of the two-

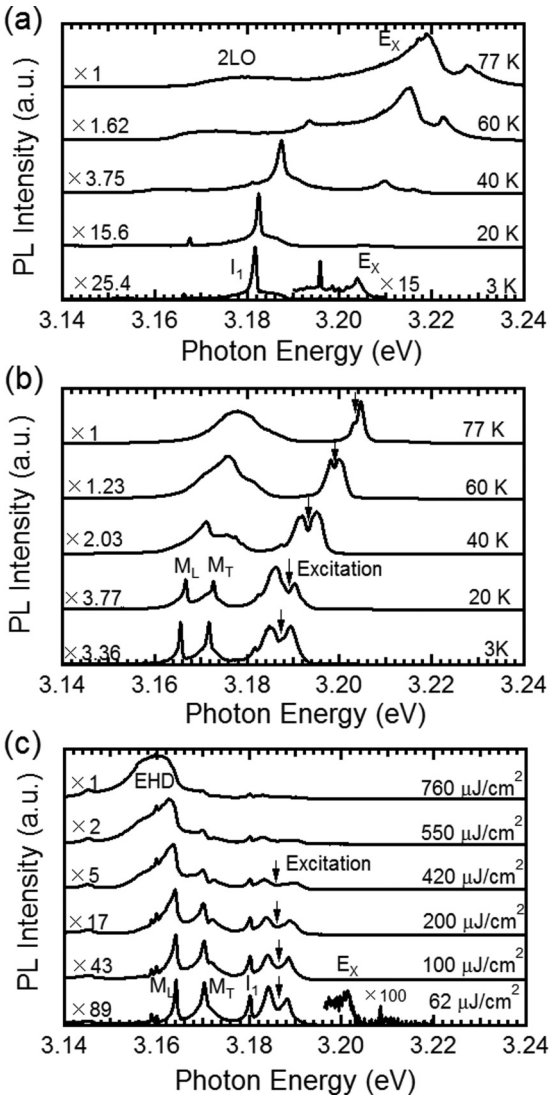

FIG. 3. Temperature dependence of PL spectra under (a) band-to-band weak excitation and (b) resonant two-photon excitation of biexcitons at 43 $\mu J/cm^2$ excitation density. E_x, I_1, and 2LO indicate the PL bands of the free exciton, the exciton trapped by the neutral accepters, and the 2LO phonon side band of the free exciton, respectively. M_T and M_L indicate the resonant two-photon Raman scattering associated with the transverse and longitudinal excitons, respectively. (c) Excitation density dependence of PL spectra under resonant two-photon excitation of biexcitons at 3 K. The arrows in (b,c) indicate the two-photon absorption energies of the biexcitons.

photon absorption band of the biexciton has been reported to be 0.26 meV at 6 K [26], and this broadened when the excitation intensity increased [27]. As the reported spectral width is sufficiently narrower than the spectral width of the excitation light, the resonant two-photon absorption energy could be recognized as a trough in the scattered excitation-light spectrum. The small width of this trough increased with increased T, because of broadening of the homogeneous width [26]. In the PL spectra, two of the resonant two-photon Raman scatterings through the biexciton state (the M_L and M_T lines, for the transverse and longitudinal excitons, respectively) and the PL bands from the biexciton state (the M_L and M_T bands)

were observed [17–19]. When T was increased, the spectral widths of the M_L and M_T lines also increased, and the M_L and M_T bands became dominant. These features are consistent with previous reports [26]. In this study, the PL bands and two-photon Raman scattering lines exhibited large spectral widths, because the spectral width of the excitation light in this experiment was larger and its peak intensity was higher than in previous reports. The results of this experiment confirm the biexciton generation by the resonant two-photon absorption process.

Figure 3(c) shows the excitation density dependence of the PL spectra at 3 K under resonant two-photon excitation of the biexcitons. When the excitation density was more than 420 μJ/cm^2, a PL band due to an electron-hole droplet (EHD) appeared at the lower-energy side of the biexciton PL band [28]. Note that an EHD is formed under resonant excitation of the excitons or resonant two-photon excitation of the biexcitons, when the exciton density is greater than the Mott density. As the presence of an EHD modifies the transient reflection spectra in the midinfrared region [28,29], it was necessary to limit the excitation density to beneath a certain threshold value. This prevented generation of an EHD, so that the IRTA spectra originating from the excitons and biexcitons could be measured. We concluded that the appropriate excitation density was significantly less than 420 μJ/cm^2.

B. Infrared transient absorption of excitons and biexcitons at 3 K

Figures 4(a)–4(e) shows the IRTA spectra for delay times of 5, 20, 50, 100, and 300 ps at 3 K. The excitation photon energy was 3.186 eV, which corresponds to the resonant two-photon absorption energy of the biexcitons. The excitation density was set to 140 μJ/cm^2 in order to suppress the EHD generation, as explained above. The obtained IRTA spectra were fit using a composition of three Gaussian functions,

$$A(E) = a_1 \exp\left[-\left(\frac{E-E_1}{b_1}\right)^2\right] + a_2 \exp\left[-\left(\frac{E-E_2}{b_2}\right)^2\right] + a_3 \exp\left[-\left(\frac{E-E_3}{b_3}\right)^2\right] + g, \quad (1)$$

where a_1,a_2, and a_3 are the peak intensities; b_1,b_2, and b_3 are the spectral widths; E_1,E_2, and E_3 are the peak energies of the three components; and g is the background. The $A(E)$ fitting curves are formatted as thick solid curves in Fig. 4(a), and each component is represented by thin curves. For the 5-ps delay time, two main peaks were observed at 168 and 184 meV (E_1 and E_3), along with a small peak at 175 meV(E_2). The two main peaks remained for a period of over 100 ps, whereas the small peak at 175 meV disappeared within several tens of picoseconds. The exciton energies of the $1s$, $2p$, and $3p$ states have been reported to be 3.202, 3.372, and 3.387 eV, respectively [16]. Consequently, the transition energies from the $1s$ to $2p$ states and those from the $1s$ to $3p$ states are expected to be 170 and 185 meV, respectively. These results are almost consistent with the observed main peak energies. The exciton lifetime was reported to be a few nanoseconds, but this is strongly dependent on the sample quality. For example, values within a range of 100−2000 ps have been reported [30]. From the IRTA decay time, which is discussed below, it was concluded that the two main peaks can be attributed to the excitons.

On the other hand, it is suggested that the small peak at 175 meV can be attributed to the biexciton transition energy. The biexciton lifetime has been reported to be 50 ps [31] under resonant two-photon absorption of the biexciton. However, it has also been reported as ranging from 30 to 67 ps [30], with slight dependence on the sample quality. The reported biexciton lifetime supports the above suggestion, because the small peak at 175 meV was annihilated within a period of several tens of picoseconds. A defined absorption peak attributable to the biexcitons was observed in CuCl bulk crystal. A previous report concerning CuCl film on a CaF_2 substrate showed a similar absorption peak for the biexcitons, but this result was ambiguous because of the low signal-to-noise ratio [21].

We next estimated the biexciton transition energy. The ratio of the biexciton binding energy to the exciton Rydberg energy was calculated as a function of the electron-to-hole effective mass ratio [9–11]. We propose that this relation can be adapted to the binding energy of the higher state. In other words, we suppose that the ratio of the binding energies of the lowest and higher states is equivalent for a hydrogen molecule and a biexciton. The binding energies of the lowest and higher states of a hydrogen molecule are approximately 4.5 and 3.5 eV [32], respectively, with a ratio of 1.37. When we adapt this value to the biexciton in CuCl, the binding energy of the $(1s, 2p)$ state is estimated to be 23 meV because the binding energy of the lowest $(1s, 1s)$ state is 32 meV. The transition energy from the $(1s, 1s)$ state to the $(1s, 2p)$ state of the biexciton is equivalent to the sum of the exciton $1s-2p$ transition energy and the difference between the biexciton energies of the $(1s, 1s)$ state and the $(1s, 2p)$ state, i.e., 9 meV. Using the experimental transition energy of the exciton $1s-2p$ states, which is 168 meV, the transition energy from the lowest $(1s, 1s)$ to the higher $(1s, 2p)$ state was calculated to be 177 eV. This energy value lies between the transition energy from the $1s$ to $2p$ exciton states and that from the $1s$ to $3p$ exciton states. Consequently, it was concluded that the small IRTA peak at 175 meV can be attributed to the biexcitons.

Figures 5(a) and 5(b) show the IRTA time profiles for probe energies of 170 and 175 meV, which correspond to the transition energies from the $1s$ to $2p$ exciton states and from the $(1s, 1s)$ to $(1s, 2p)$ biexciton states, respectively. The experimental time profile was composed of two decay components (fast and slow). Therefore, we fit the time profiles according to

$$F(t) = c_1 \exp\left[-\left(\frac{t}{\tau_1}\right)\right] + c_2 \exp\left[-\left(\frac{t}{\tau_2}\right)\right], \quad (2)$$

where t is time, c_1 and c_2 represent the transient absorption intensities, and τ_1 and τ_2 represent the decay times of the fast- and slow-decay components, respectively. From the fitting results for 170-meV probe energy, τ_1 and τ_2 were obtained as 8.9 ± 2.0 and 160 ± 10 ps, respectively. This means that the exciton exhibited two relaxation processes. On the other hand, for the 175-meV photon energy, τ_1 and τ_2 values of 17.6 ± 2.0

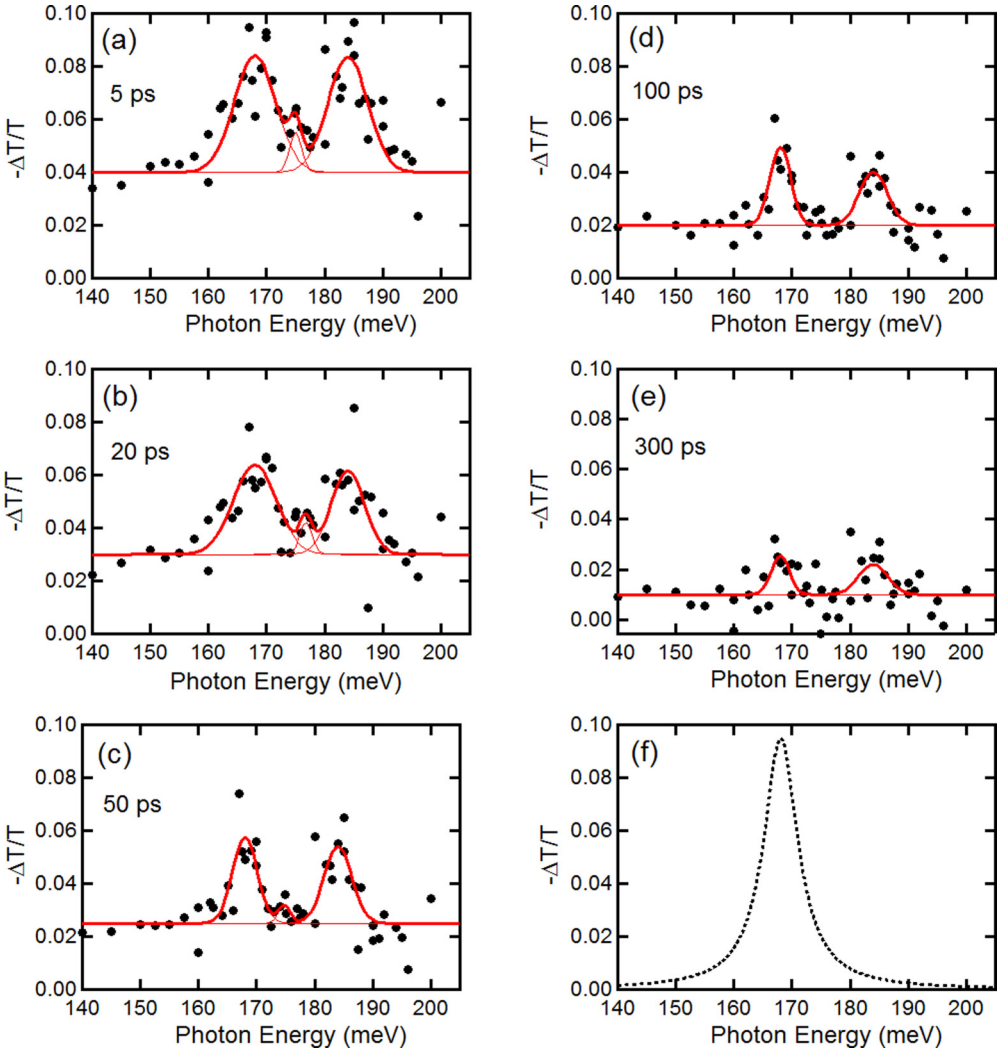

FIG. 4. IRTA spectra at 3 K for the delay time of (a) 5, (b) 20, (c) 50, (d) 100, and (e) 300 ps. The thin solid curves represent the fitting results for the three Gaussian functions considering the three absorption bands due to the exciton $1s-2p$ state, $1s-3p$ state, and the biexciton $(1s, 1s-1s, 2p)$ state transitions, respectively. The thick solid curves are the sums of the three fitting curves. (f) Absorption spectra for exciton $1s-2p$ states calculated using Eq. (4).

and 186 ± 14 ps, respectively, were obtained. The fast-decay component was attributed to the biexciton decay. Further, as the transient absorption peak intensity of the biexciton was smaller than the exciton peak, the exciton contribution to the time profiles was included as the slow-decay component. As it is possible for the slow decay times of both photon energies to be equivalent, it was concluded that the slow-decay components were due to the excitons as described above. On the other hand, the fast relaxation of the excitons with 8.9-ps decay time indicates the possible existence of a certain nonradiative relaxation process. The I_1 line is strongest in the PL spectra; therefore it may originate from the trapping process due to the impurities.

In the case of ideal resonant two-photon excitation of the biexcitons, excitons are generated as a result of biexciton annihilation. Therefore, an exciton formation time should be apparent in the time profiles; however, this was not defined in our experiment. In fact, the transient absorption peaks were observed clearly for 5-ps delay time. The reasons why the excitons were generated immediately are as follows. First, one-photon absorption of the excitons occurred due to the absorption band tail. Second, unexpectedly fast exciton generation occurred via a biexciton-biexciton scattering process, which resulted from the high biexciton density. The biexciton-biexciton scattering process induced a decrease in the biexciton lifetimes. As the fast-component decay time of 17.6 ± 2.0 ps obtained here is shorter than the reported biexciton lifetime, this suggests that biexciton-biexciton scattering occurs. The two possibilities described above are independent from each other, and the expected time profiles are different. However, it is difficult to distinguish between them in the obtained time profiles, so the contribution to the fast-decay component remains ambiguous.

Finally, the origin of the background g in the fitting results is discussed. In Fig. 5(c), a_1, a_2, a_3, and g, which were obtained by the fitting results with Eq. (1) for the IRTA spectra, were plotted as a function of the delay time. As discussed above, a_1 and a_3 are attributed to the peak intensities of

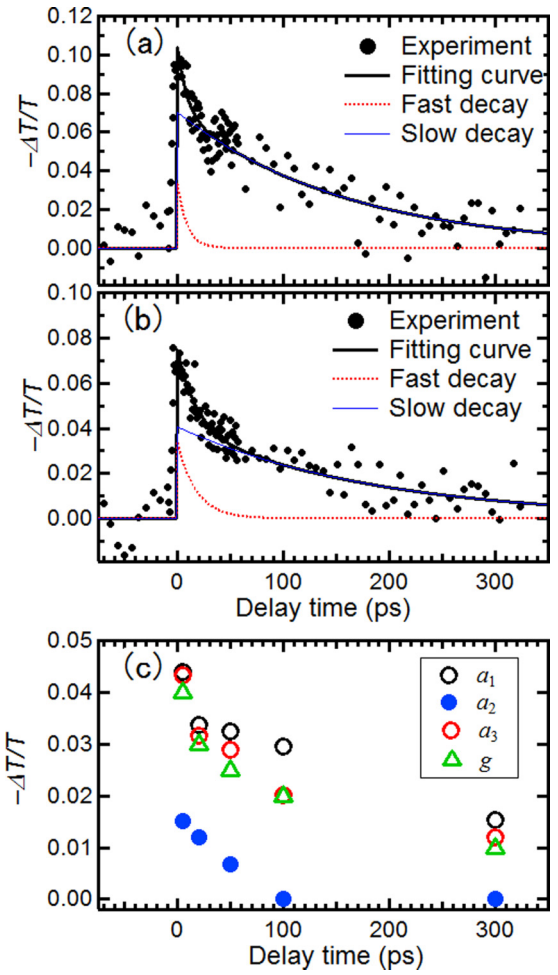

FIG. 5. IRTA time profiles at (a) 170 and (b) 175 meV at 3 K. The experimental results were fit using Eq. (2). The dotted and solid curves are the fast- and slow-decay components, respectively, and the thick solid curves are their sums. (c) Fitting parameters a_1,a_2,a_3, and g as a function of the delay time, which were obtained from fitting the results to the IRTA spectra, as expressed in Fig. 4.

the exciton's transitions due to $1s-2p$ states and $1s-3p$ states, respectively, and a_2 is attributed to the peak intensity of the biexciton's transition due to $(1s,\ 1s-1s,\ 2p)$ states. Since the decays of a_1,a_3, and g were almost the same, it is concluded that the background g is also associated with the excitons. Their decays comprised a combination of the small instantaneous decay and the main slow decay. The time profile at 170 meV is composed of a_1 and g. On the other hand, the intensity of a_2 disappeared in less than 100 ps, which corresponds to the fast-decay component, mainly in the time profiles at 175 meV. According to the fitting results in Figs. 4(a)–4(f), the slow-decay component is due to the background g.

The IRTA component of g can be attributed to the transition between the internal energy levels of the excitons because of its energy range. Since the binding energy to the impurities was- about several tens of milli-electron-volts, exciton dissociation from the impurities is neglected. It is suggested that the ambiguous IRTA spectrum assigned as g is due to the transitions of the internal levels of the excitons

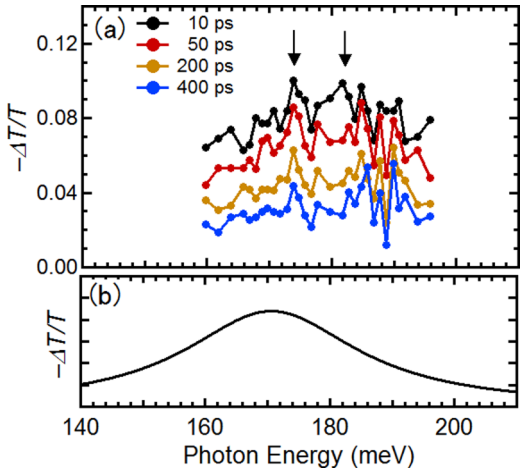

FIG. 6. (a) Transient absorption spectra for different delay times of 10, 50, 200, and 400 ps at 77 K. The downward arrows indicate the photon energies of the time profiles shown in Fig. 7. (b) Absorption spectra of exciton $1s-2p$ states calculated using Eq. (4).

trapped by the impurities. Since the wave function of an electron-hole pair bound to an impurity is modified from a free exciton, it is reasonable to consider that the transition peaks due to the internal energy levels of the exciton, which result from the relative motion of an electron and a hole, disappeared and resulted in a broad background. Another candidate inducing the continuous absorption spectrum is the free carriers; photoexcited free carriers appeared as an EHD in this experiment. However, the excitation density was low to suppress the generation of the EHD. In addition, the lifetime of the EHD is very short compared to that of the excitons. Consequently, we concluded that the IRTA component of g is attributed to the bound excitons. In the transient absorption measurement, it is difficult to distinguish the contributions due to the free and bound excitons, unless their decay times are clearly different. However, it is thought that the giant oscillator strength shortens the radiative time of the bound exciton compared to that of the free excitons.

C. Infrared transient absorption of excitons and biexcitons at 77 K

Figure 6(a) shows the IRTA spectra for each examined delay time (10, 50, 200, and 400 ps) at 77 K, where the range of the horizontal axis is the same that of Fig. 4. In contrast to the IRTA spectra in Figs. 4(a)–4(e), definite peaks disappeared, and very broad spectra were obtained. These broad IRTA spectra remained for delay times of more than 400 ps; thus we concluded that they are attributed to the excitons. As discussed later, we concluded that the large damping rate of the excited states of the exciton and biexciton results in the disappearance of the peaks. In order to examine the contributions of the excitons and biexcitons to the IRTA spectra, the time profiles were analyzed. The photon energy for the maximum of the IRTA, 174 meV, and its 8-meV-higher energy, 182 meV, were selected to analyze the time profiles, where the 8-meV energy separation was almost consistent with the energy separation between the biexciton's transition due to $(1s,\ 1s-1s,\ 2p)$ states and the exciton's transition due to $1s-2p$ states.

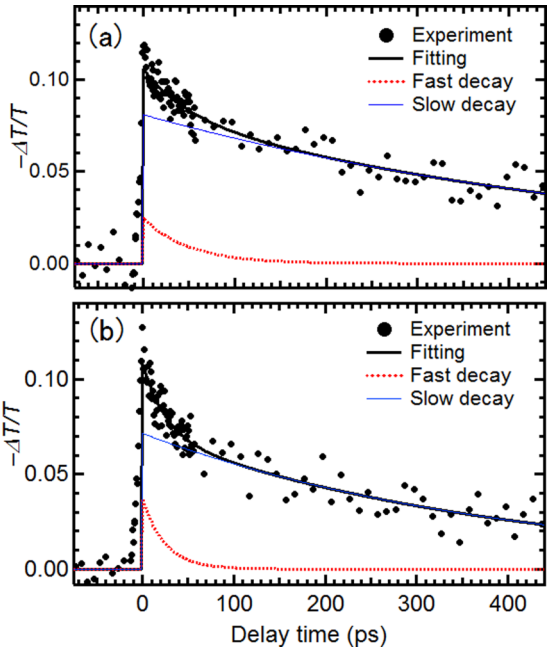

FIG. 7. IRTA time profiles at (a) 174- and (b) 182-meV probe photon energies at 77 K. The experimental results were fit using double exponential functions. The dotted and solid curves are the fast- and slow-decay components, respectively, and the thick solid curves are their sums.

Figures 7(a) and 7(b) show the IRTA time profiles at probe energies of 174 and 182 meV, respectively, at the same T. The time profiles were fit using Eq. (2). At 174 meV, τ_1 and τ_2 were obtained as 49 ± 27 and 583 ± 123 ps, respectively, whereas at 182 meV, τ_1 and τ_2 values of 25 ± 9 and 393 ± 53 ps were obtained, respectively. The slow-decay components for both probe photon energies were attributed to the free excitons. At 3 K, the fast-decay components were attributed to the biexciton's decay or the trapping process of the exciton to the impurities. However, at 77 K, the disappearance of the definite peaks made it difficult to distinguish them. The values of τ_1 at 174 meV are greater than τ_1 at 170 meV at 3 K. This implies that the trapping rate of the free excitons decreased with increasing T. On the other hand, the difference between τ_1 at 182 meV at 77 K and that at 175 meV at 3 K was not clear. Since the biexciton's decay was determined not by the intrinsic lifetime but by the biexciton-biexciton scattering process, it is reasonable that the decay time was not changed drastically. However, from the results that all IRTA peaks disappeared and only the broad spectra remained, it is impossible to distinguish the contributions of the biexciton's decay and the exciton's trapping process in the fast-decay components. We suggest that the spectral broadening for both the exciton's and biexciton's transitions with increasing T results in a mixture of their contributions. On the other hand, the slow-decay components were due to the excitons: the free excitons and the excitons trapped to the impurities. The decay time τ_2 at 77 K is greater than that at 3 K. This originates from the fact that the contributions of the free excitons became dominant with increasing T.

In addition, we examined the IRTA spectrum due to the transition from the $1s$ to $2p$ exciton states, along with its T dependence. The IRTA spectrum $N(E)$ considering the thermal distribution of the exciton and the differences in the effective masses of the $1s$ and $2p$ excitons [3] can be expressed as

$$N(E,T) \propto \sqrt{\frac{E - E_{1s-2p}}{m_{1s}/m_{2p} - 1}} \exp\left[-\frac{E - E_{1s-2p}}{k_B T(m_{1s}/m_{2p} - 1)}\right], \quad (3)$$

where m_{1s} and m_{2p} are the center of masses of the $1s$ and $2p$ excitons, respectively, E_{1s-2p} is the energy difference between the $1s$ and $2p$ states at a wave number k of 0, and k_B is the Boltzmann constant. Note that m_{1s} and m_{2p} have been reported as $2.3m_0$ [33] and $2.071m_0$ [34], respectively, where m_0 is the electron mass at rest. E_{1s-2p} was 168 meV, as obtained from the experimental results. In addition, through convolution using a Lorentz function reflecting the homogeneous broadening of the transition, we calculated the IRTA spectrum $S(E,T)$, such that

$$S(E,T) = \int_{-\infty}^{\infty} N(E,T) \frac{A}{(E - E')^2 - \Gamma(T)^2} dE', \quad (4)$$

where A is an arbitrary constant. To evaluate the damping constant $\Gamma(T)$, the T dependence of the exciton absorption bands was measured from the two-photon excitation spectra of the I_1 line. Figure 8(a) shows the two-photon excitation spectra from 3 to 50 K. We observed the absorption bands of the $1s$, $2p$, and $3p$ states, 1LO phonon sideband of the $2p$ state of the Z_3 exciton, and the absorption band of the $1s$ state of the $Z_{1,2}$ exciton. The absorption bands due to the $2p$ and $3p$ states broadened with increasing T and disappeared at T values greater than 50 K. These absorption bands were extracted through subtraction of the continuous base, and the full width at half maximum (FWHM) values of the bands were obtained by fitting to the Lorentz function with deconvolution of the excitation-light spectrum, as shown in Fig. 8(b).

Here, we examine the T dependence of the peak energies of the two-photon absorption bands, which are shown in Fig. 8(c). The peak energy of the Z_3 $1s$ exciton, which is 3.210 eV at 10 K, does not agree with the transverse $1s$ exciton energy, being 3.204 eV, which was determined via the PL spectrum. As the transverse $1s$ exciton is optically forbidden under the two-photon absorption process, we suggest that violation of the selection rule occurs for an energy higher than the resonant energy of the one-photon process. The $2p$, $3p$, and $2p + \mathrm{LO}$ bands exhibit the same energy shifts as a function of T. That is, with increased T up to 20 K, the peak energy shifts to the lower-energy side. When T surpassed 20 K, the peak energy begins to increase. As a reference, the T dependence of the PL peak energy of the I_1 line is also expressed in the figure, the energy shift of which corresponds to a change in the band-gap energy. In comparison with this result, it was concluded that the blueshift of the $2p$ exciton band at T values of more than 20 K is due to the band-gap energy. On the other hand, the reason why the $2p$ band exhibits a redshift for T values of up to 20 K has not been revealed. At low T, another condition must be considered, in addition to the change in the band-gap energy, which is related to the transition probability of the two-photon absorption process. In the previous report

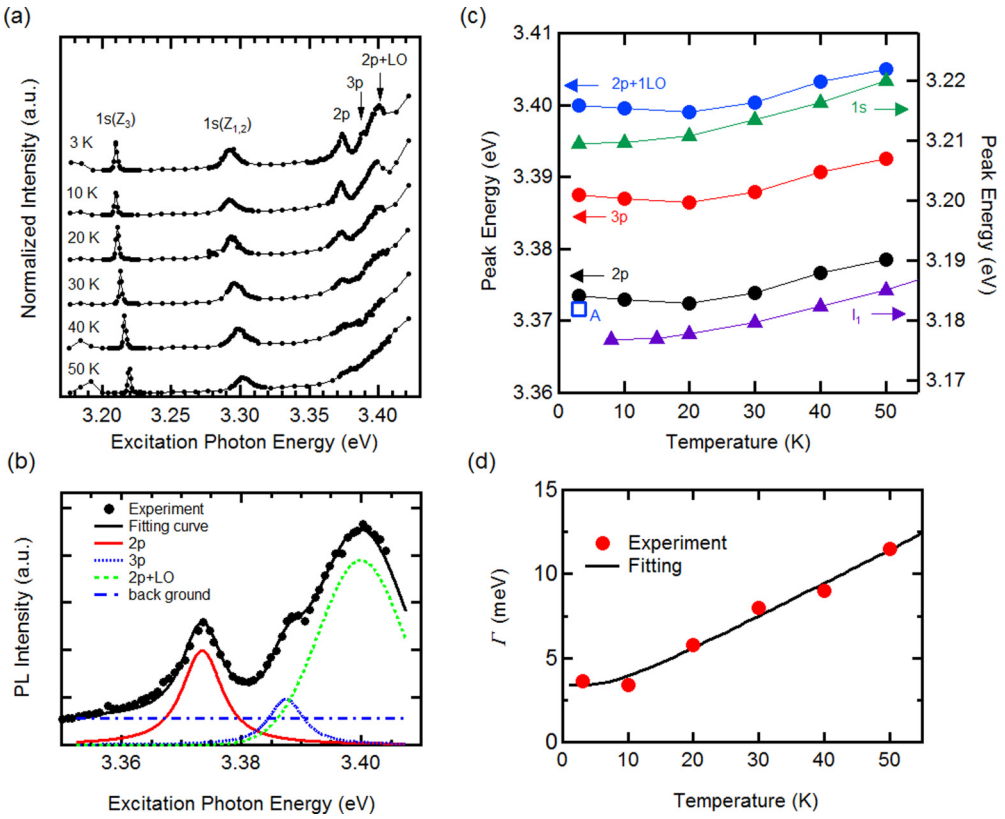

FIG. 8. (a) Two-photon PL excitation spectra of I_1 line from 3 to 50 K. (b) Experimental PLE spectrum at 3 K (solid circles) and fitting curves considering absorption bands of $2p$, $3p$, and LO-phonon sideband of the Z_3 excitons. (c) Temperature dependence of peak energies in PLE spectra. The $2p$, $3p$, and $2p + 1$LO energies of the Z_3 exciton are associated with the left axis and the $1s$ energy of the same exciton is associated with the right axis. The $2p$ exciton energy measured in the previous report [16] is marked as A. In addition, the PL peak energy of the I_1 line is shown. (d) Temperature dependence of $2p$-band spectral width. The solid circles indicate the experimental results and the solid curve is the fitting curve obtained from Eq. (5).

by Saito *et al.* [16], the $2p$ exciton energy was reported to be 3.3717 eV at 3 K, which is lower than the experimental value obtained in this study. Therefore, the redshift observed in this study may be an extrinsic property of our sample, for example, a strain effect. Consequently, the transition energy for the exciton $1s - 2p$ state transition obtained from the IRTA is inconsistent with the energy separation between the $1s$ and $2p$ states determined from the PLE spectra. Therefore, we consider the T dependence of the IRTA spectra in terms of the damping constant and its T dependence. Figure 8(d) shows the T dependence of the spectral width of the $2p$ absorption band, where the experimental data were fit using Eq. (5) [35]. The damping constant is expressed as

$$\Gamma(T) = \Gamma_0 + \frac{E_a}{\exp(E_b/k_B T) - 1}, \tag{5}$$

and the experimental results could be well reproduced using $\Gamma_0 = 3.37$ meV, $E_a = 4.41$ meV, and $E_b = 1.88$ meV. Γ_0 represents the intrinsic damping constant, and E_a and E_b phenomenologically correspond to the interaction energy with the phonons and the activation energy of the interaction, respectively. The IRTA spectra due to the transition from the exciton $1s$ to $2p$ states were calculated using Eq. (4), along with the spectral widths of the $1s$ and $2p$ bands of the Z_3 exciton.

The IRTA spectrum calculated for $T = 3$ K is shown in Fig. 4(f). Note that the spectral widths were inconsistent. For the experimental IRTA spectra, the spectral width decreased with time evolution. As the possibility exists that the excitons are generated by nonelastic scattering between the biexcitons, as mentioned above, it is suggested that the spectral width at 5-ps delay time reflects the effective temperature of the $1s$ exciton, which is higher than the sample temperature. Further, the cooling process of the $1s$ excitons results in narrowing of the spectral width with time evolution. However, the spectral width of the calculated IRTA spectrum is larger than that of the experimental IRTA spectrum at 100-ps delay time. Thus it is thought that the excitation-light power was sufficiently strong to extend the homogeneous width of the $2p$ exciton. The spectral width of our calculated result was 7.3 meV. However, in the previous report [16], the spectral width of the exciton $2p$ absorption band was less than 5 meV, which was almost consistent with our experimental result at 100-ps delay time. From these considerations, it is reasonable to conclude that the IRTA spectra were determined by the homogeneous width of the $2p$ band. As regards the results at 77 K, Γ was obtained as 34 meV by extrapolating from the fitting result. The calculated result, which is shown in Fig. 6(b), did not agree well with the experimental result. However, the quite large spectral width was well reproduced. This result indicates that the very wide

background obtained for the long decay time was due to the excitons. The difference in the effective masses of the $1s$ and $2p$ exciton states is expected to result in a blueshift in the transition peak energy and the spectral broadening. In this experiment, however, broadening of the spectral width of the $2p$ exciton band determined the IRTA spectra, because the homogeneous width of the $2p$ exciton band also increased.

IV. SUMMARY

We observed the exciton optical transitions from the lowest $1s$ to the higher $2p$ states in a CuCl single crystal. In addition, the optical transition of the biexcitons from the lowest ($1s$, $1s$) to the higher ($1s$, $2p$) states was also observed. The excited-state energy of the ($1s$, $2p$) state of the biexciton agreed with the energy value estimated by considering the binding energy ratio of a hydrogen molecule. In addition, the abrupt broadening of the $2p$ exciton absorption band with increasing T was found to cause the disappearance of the fine structures of the IRTA spectra. Our findings are significant, because optical phenomena originating from the internal energy levels of the exciton are associated with excitonic coherent phenomena. Furthermore, observation of the biexciton excited states in a semiconductor will advance the study of multiexciton properties with regard to the generation of nonlinear optical phenomena.

ACKNOWLEDGMENTS

We wish to express our gratitude to Professor Tadashi Itoh and Masaaki Ashida of Osaka University for valuable advice on our experimental procedures. We also wish to thank Dr. Junko Usukura and Professor Eiji Tokunaga at the Tokyo University of Science, along with Professor S. Nair of Toronto University, for helpful suggestions regarding the biexciton binding energy.

[1] M. Ueta, H. Kanzaki, K. Kobayashi, Y. Toyozawa, and E. Hamamura, *Excitonic Processes in Solids* (Springer-Verlag, Berlin, 1984).
[2] M. Kuwata-Gonokami, M. Kubouchi, R. Shimano, and A. Mysyrowicz, J. Phys. Soc. Jpn. **73**, 1065 (2004).
[3] T. Tayagaki, A. Mysyrowicz, and M. Kuwata-Gonokami, J. Phys. Soc. Jpn. **74**, 1423 (2005).
[4] D. Fröhlich, A. Nöthe, and K. Reimann, Phys. Rev. Lett. **55**, 1335 (1985).
[5] S. Leinß, T. Kampfrath, K. v. Volkmann, M. Wolf, J. T. Steiner, M. Kira, S. W. Koch, A. Leitenstorfer, and R. Huber, Phys. Rev. Lett. **101**, 246401 (2008).
[6] T. Kazimierczuk, D. Fröhlich, S. Scheel, H. Stolz, and M. Bayer, Nature **514**, 343 (2014).
[7] M. Wagner, H. Schneider, D. Stehr, S. Winnerl, A. M. Andrews, S. Schartner, G. Strasser, and M. Helm, Phys. Status Solidi B **248**, 859 (2011).
[8] M. Wagner, M. Teich, M. Helm, and D. Stehr, Appl. Phys. Lett. **100**, 051109 (2012).
[9] O. Akimoto and E. Hanamura, J. Phys. Soc. Jpn. **33**, 1537 (1972).
[10] W.-T. Huang, Phys. Status Solidi B **60**, 309 (1973).
[11] W. F. Brinkman, T. M. Rice, and B. Bell, Phys. Rev. B **8**, 1570 (1973).
[12] G. H. Dieke, J. Mol. Spectrosc. **2**, 494 (1958).
[13] J. Faist, F. Capasso, C. Sirtori, D. L. Sivco, A. L. Hutchinson, M. S. Hybertsen, and A. Y. Cho, Phys. Rev. Lett. **76**, 411 (1996).
[14] B. F. Levine, K. K. Choi, C. G. Bethea, J. Walker, and R. J. Malik, Appl. Phys. Lett. **50**, 1092 (1987).
[15] T. Uozumi and Y. Kayanuma, Phys. Rev. B **65**, 165318 (2002).
[16] K. Saito, M. Hasuno, T. Hatano, and N. Nagasawa, Solid State Commun. **94**, 33 (1995).
[17] G. M. Gale and A. Mysyrowicz, Phys. Rev. Lett. **32**, 727 (1974).
[18] S. Suga and T. Koda, Phys. Status Solidi B **61**, 291 (1974).
[19] B. Hönerlage, V. D. Phach, and J. B. Grun, Phys. Status Solidi B **88**, 545 (1978).
[20] K. Miyajima, M. Ashida, and T. Itoh, J. Phys.: Condens. Matter **19**, 445006 (2007).
[21] T. Yoshioka, K. Miyajima, M. Ashida, and T. Itoh, Phys. Status Solidi C **6**, 296 (2009).
[22] K. Yamanaka, K. Edamatsu, and T. Itoh, J. Lumin. **87-89**, 312 (2000).
[23] T. Ikehara and T. Itoh, Phys. Rev. B **44**, 9283 (1991).
[24] W. Staude, Phys. Status Solidi B **43**, 367 (1971).
[25] A. Göbel, T. Ruf, M. Cardona, C. T. Lin, J. Wrzesinski, M. Steube, K. Reimann, J.-C. Merle, and M. Joucla, Phys. Rev. B **57**, 15183 (1998).
[26] T. Itoh, S. Watanabe, and M. Ueta, J. Phys. Soc. Jpn. **48**, 542 (1980).
[27] T. Itoh and T. Katohno, J. Phys. Soc. Jpn. **51**, 707 (1982).
[28] M. Nagai and M. Kuwata-Gonokami, J. Lumin. **100**, 233 (2002).
[29] M. Nagai, R. Shimano, and M. Kuwata-Gonokami, Phys. Rev. Lett. **86**, 5795 (2001).
[30] T. Ikehara and T. Itoh, Solid State Commun. **79**, 755 (1991).
[31] H. Akiyama, T. Kuga, M. Matsuoka, and M. Kuwata-Gonokami, Phys. Rev. B **42**, 5621 (1990).
[32] R. S. Mulliken, Rev. Mod. Phys. **4**, 1 (1932).
[33] T. Mita, K. Sotome, and M. Ueta, Solid State Commun. **33**, 1135 (1980).
[34] B. Ghebouli, M. A. Ghebouli, M. Fatmi, T. Chihi, Z. Heiba, and S. Boucetta, Chin. J. Phys. **51**, 738 (2013).
[35] Y. Masumoto, T. Wamura, and A. Iwaki, Appl. Phys. Lett. **55**, 2535 (1989).